arXiv:1611.04282v1 [astro-ph.SR] 14 Nov 2016

Amplitude of solar wind density turbulence from 10–45 $R_\odot$

K. Sasikumar Raja[1*], Madhusudan Ingale[1†], R. Ramesh[2], Prasad Subramanian[1‡], P. K. Manoharan[3]and P. Janardhan[4]

[1]Indian Institute of Science Education and Research, Pashan, Pune - 411 008

[2]Indian Institute of Astrophysics, 2nd Block, Koramangala, Bangalore - 560 034

[3]Radio Astronomy Centre, National Centre for Radio Astrophysics, Tata Institute of Fundamental Research, Udhagamandalam (Ooty) - 643 001

[4]Physical Research Laboratory, Navrangpura, Ahmedabad - 380 009

Key Points:

- How do the solar wind density modulation index and turbulence amplitude vary with heliocentric distance and sunspot number?
- Is the large scale coronal magnetic field linked to solar wind density turbulence?

*Indian Institute of Science Education and Research, Pashan, Pune - 411 008

†Currently at Physical Research Laboratory, Navrangpura, Ahmedabad - 380 009

‡Also Centre for Excellence in Space Sciences, India. http://www.cessi.in

Corresponding author: K. Sasikumar Raja, sasikumar@iiserpune.ac.in

Abstract

We report on the amplitude of the density turbulence spectrum (C_N^2) and the density modulation index ($\delta N/N$) in the solar wind between 10 and $45R_\odot$. We derive these quantities using a structure function that is observationally constrained by occultation observations of the Crab nebula made in 2011 and 2013 and similar observations published earlier. We use the most general form of the structure function, together with currently used prescriptions for the inner/dissipation scale of the turbulence spectrum. Our work yields a comprehensive picture of a) the manner in which C_N^2 and $\delta N/N$ vary with heliocentric distance in the solar wind and b) of the solar cycle dependence of these quantities.

1 Introduction

The extended solar corona and the solar wind is a rich testbed for studying the properties of magnetohydrodynamic (MHD) turbulence. While most solar wind turbulence theories only treat incompressible turbulence, density irregularities are present in the solar wind, and are manifested through fluctuations in the refractive index. Knowledge of density turbulence impacts our understanding of the solar wind significantly, and is important for interpreting a variety of observations. It is linked to our basic understanding of the compressibility of solar wind turbulence (e.g., *Tu and Marsch* [1994]; *Hnat et al.* [2005]). It is also key to infer radio wave scattering leading to depressed quiet Sun brightness temperatures at low radio frequencies [*Thejappa and Kundu*, 1992; *Sastry*, 1994; *Ramesh*, 2000a; *Subramanian*, 2004; *Ramesh et al.*, 2006; *Thejappa and MacDowall*, 2008], the dissipation of solar wind turbulence, leading to extended solar wind heating (e.g., *Carbone et al.* [2009]; *Chandran et al.* [2009]), energetic particle propagation through the heliosphere (e.g., *Reid and Kontar* [2010]) and other interesting problems.

Density turbulence in solar wind has been studied using techniques ranging from angular broadening of radio sources (e.g., *Armstrong et al.* [1990]; *Janardhan and Alurkar* [1993]; *Anantharamaiah et al.* [1994]; *Bastian* [1994]; *Spangler and Sakurai* [1995]; *Ramesh et al.* [2001]) to spectral broadening [*Coles and Harmon*, 1989], phase scintillations [*Woo and Armstrong*, 1979], interplanetary (intensity) scintillations (IPS) [*Hewish et al.*, 1964; *Cohen and Gundermann*, 1969; *Ekers and Little*, 1971; *Rickett*, 1990; *Manoharan et al.*, 2000; *Bisi et al.*, 2009, 2010; *Tokumaru et al.*, 2012, 2016] due to celestial radio sources and spacecraft radio beacons [*Imamura et al.*, 2014]. Despite this impressive body of work, there are still significant gaps in our understanding. For instance: while the spatial spectrum of density turbulence is gen-

erally acknowledged to follow the Kolmogorov scaling at relatively large scales, there is evidence for flattening of the spectrum near the inner/dissipation scale (e.g., *Coles and Harmon* [1989]; *Coles et al.* [1991]). The location of the inner/dissipation scale is also a subject of considerable uncertainty. Another important quantity of interest is the so-called density modulation index $\delta N/N$, where δN represents the turbulent density fluctuations and N represents the background solar wind density. There have been some past attempts at measuring this quantity [*Woo et al.*, 1995; *Bavassano and Bruno*, 1995; *Spangler*, 2002] and a relatively recent comprehensive study for heliocentric distances $> 40R_{\odot}$ using the IPS technique [*Bisoi et al.*, 2014a].

Some of the uncertainties in our understanding of solar wind density turbulence are manifested in the debate regarding the smallest observable source in the solar corona at radio wavelengths. Since coronal turbulence broadens the source size, observations of compact sources place limits on the spectral amplitude of density turbulence. Observations reported by *Lang and Willson* [1987]; *Zlobec et al.* [1992]; *Mercier et al.* [2006, 2015] at $\approx$ 327 MHz with angular resolutions < 10 arc sec suggest that the smallest coronal radio source size is ≥ 30 arc sec. Source sizes estimated from majority of the high angular resolution observations at lower frequencies ($\approx$ 30-100 MHz) also seem to be limited to ≥ 60 arc sec [*Willson et al.*, 1998; *Ramesh et al.*, 1999; *Ramesh and Sastry*, 2000b; *Ramesh and Ebenezer*, 2001; *Ramesh et al.*, 2012; *Mugundhan et al.*, 2016], consistent with the predicted minimum observable source sizes in this frequency range [*Riddle*, 1974; *Cairns*, 2004]. However, much smaller coronal radio sources have also been reported at $\approx$ 170 MHz [*Kerdraon*, 1979; *Kathiravan et al.*, 2011]. Generally, the consensus is that scatter-broadened source sizes in the solar corona are most likely ≥ 10 arc sec at 20 cm [*Bastian*, 1994] and ≥ 3 arc min at 100 MHz [*Bastian*, 2004]. This therefore emphasizes the need for reliable estimates of the amplitude of density turbulence at these scales, especially as a function of heliocentric distance.

In this work, we will use interferometric observations of the Crab nebula to infer the spectral level of solar wind density turbulence and the density modulation index as a function of heliocentric distance. Crab occultation is a very well established technique that has been in use since the 1950s [*Hewish*, 1957, 1958; *Hewish and Wyndham*, 1963; *Erickson*, 1964; *Sastry and Subramanian*, 1974], giving us the advantage of a standard observational quantity to draw inferences from. The schematic diagram of the occultation is shown in Figure 1. This technique is also best suited for turbulence density estimates in the $\approx 10-50\ R_{\odot}$ heliocentric distance range. The IPS technique at low frequencies usually probes heliocentric distances $> 40 - 50\ R_{\odot}$. IPS observations at microwave frequencies probe the inner solar wind [*Ek-*

ers and Little, 1971; *Yamauchi et al.*, 1998a; *Imamura et al.*, 2014]. Nonetheless, extensive studies of density turbulence amplitude and density modulation index and their solar cycle dependence were still lacking.

We have used Crab occultation observations made in 2011 and 2013 at the Gauribidanur observatory [*Ramesh*, 2011], together with published data from several earlier observations by *Machin and Smith* [1952]; *Hewish* [1957, 1958]; *Hewish and Wyndham* [1963] over the interferometer baselines $60-1000$ meters and frequencies $26-158$ MHz. We have scaled these measured structure functions to a baseline of 1600 meters and a frequency of 80 MHz, which were the parameters corresponding to Crab occultation observations in 2011 and 2013.

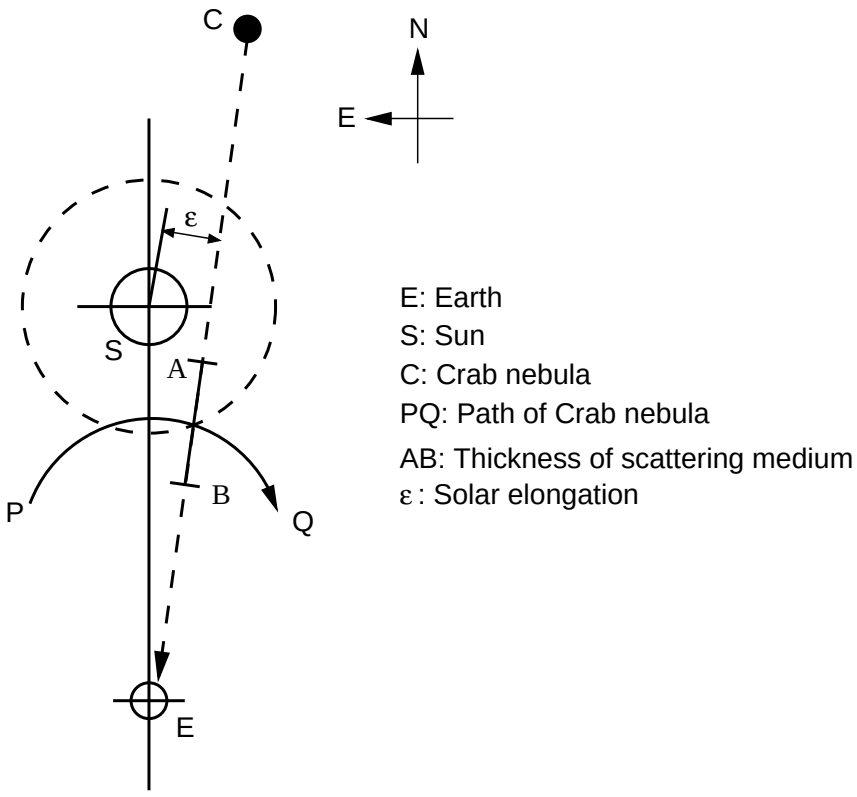

Figure 1. The schematic diagram shows the geometry of Crab nebula occultation; 'PQ' indicates the projected path of the Crab nebula during the month of June. The closest point of 'PQ' to 'S' is $\approx 5\ R_{\odot}$. The radiation from the 'C' passes through the effective turbulent medium 'AB' at a solar elongation of 'ϵ' as viewed from 'E'.

2 Density turbulence: some background

Turbulent density inhomogeneities in the solar corona are typically characterized by their spatial power spectrum

$$P_{\delta N}(k) = C_N^2(R) k^{-\alpha} e^{-(k l_i(R)/2\pi)^2}\,, \tag{1}$$

where k is the (isotropic) wave number, and $l_i(R)$ is the inner (dissipation) scale, where the spectrum steepens. The quantity C_N^2 is the amplitude of density fluctuations, and has dimensions of $\mathrm{cm}^{-\alpha-3}$. There are not many estimates of C_N^2 in the literature; for example $C_N^2(R)$ is estimated using in-situ observations of Helios [*Marsch and Tu,* 1990] and VLBI observations [*Sakurai*, 1993; *Spangler and Sakurai*, 1995; *Spangler et al.*, 1996]. Using VLBI observations of phase scintillations, *Spangler and Sakurai* [1995]; *Spangler et al.* [1996] empirically quantified the dependence of C_N^2 on heliocentric distance as

$$C_N^2(R) = 1.8 \times 10^{10} (R/10)^{-3.66} \tag{2}$$

over $R \approx 10 - 60\ R_\odot$. They assumed a Kolmogorov spectrum ($\alpha = 11/3$) for the density fluctuation, and the units of C_N^2 in Eq 2 are $m^{-20/3}$. We note that the spatial scales of the density inhomogeneities probed using VLBI are $\approx 200{-}2000$ km, which are substantially larger than the scales we are interested in ($\leq$ 10 km). To the best of our knowledge, our work provides the only parametrisation of the density turbulence amplitude as a function of heliocentric distance since *Spangler and Sakurai* [1995]; *Spangler et al.* [1996].

Another important quantity of interest to us is the magnitude of the turbulent density fluctuations δN_{k_i} at the inner scale (l_i), which can be related to the spatial power spectrum (Eq 1) as follows [*Chandran et al.*, 2009]:

$$\delta N_{k_i}^2(R) \sim 4\pi k_i^3 P_{\delta N}(R, k_i) = 4\pi C_N^2(R) k_i^{3-\alpha} e^{-1}\,, \tag{3}$$

where we have used $k_i \equiv 2\pi/l_i$. Eq (3) can be used to calculate the density modulation index $\epsilon_N(R)$ defined as

$$\epsilon_N(R) \equiv \frac{\delta N_{k_i}(R)}{N(R)}\,, \tag{4}$$

where N is the solar wind background density.

3 Observations, structure function and the scattering measure

We now briefly describe the Crab occultation observations and detail how we obtain the structure function and scattering measure from the measurements. These quantities will be used to compute C_N^2 (Eq 1) and ϵ_N (Eq 4)

3.1 Crab occultation observations

Since the Crab occultation technique is a well established one, we only briefly mention the aspects essential to our purpose. The Crab nebula is usually observed with a single element interferometer as it passes through the solar wind from $\approx$ 10–45 $R_\odot$ during mid June of every year. As it gets close to the Sun, its angular size increases due to enhanced scattering by the solar wind turbulent density irregularities. Eventually, its size increases to such an extent that it gets resolved out by the interferometer; the interferometer visibility decreases to unobservable levels, causing it to appear "occulted".

The lower panel of Figure 2 shows the variation in the observed flux density of the Crab nebula during June 2011 and 2013; while the upper panel shows the solar disk view of the occultation geometry. While there is a steady decrease in the observed flux density (from the pre-occultation value of $\approx 2015 \pm 100$ Jy) from 10th June ($R \approx 23\ R_\odot$) during the ingress in 2011, the decrease is noticeable from 8th June onwards ($R \approx 30\ R_\odot$) in 2013 (see Figure 2). A similar situation occurs during the egress. While the pre-occultation value is reached around 21st June ($R \approx 21\ R_\odot$) in 2011, it is only around 23rd June ($R \approx 29\ R_\odot$) in 2013. No fringes were observed during $12-18$ June in both 2011 and 2013. The distance of the line-of-sight to the Crab nebula from the Sun, was $R \approx 15\ R_\odot$ on 12th June (ingress) and was $R \approx 10\ R_\odot$ on 18th June (egress). Considering the fact that the heliographic latitudes encountered by the Crab nebula during the ingress and egress are different [*Kundu*, 1965], we find that the occultation curves for the years 2011 and 2013 in Figure 2 are fairly symmetric. This is expected since the maximum of the solar cycle 24 was in the year 2013 and it has been shown that distribution of solar wind density fluctuations is spherically symmetric close to the solar maximum [*Manoharan*, 1993].

In the present work, we have used these observations as well as similar ones made earlier. Crab nebula occultation observations were reported by *Machin and Smith* [1952] in 1952 at 38 and 80.5 MHz. Similar observations during 1952-1958 were reported in *Hewish* [1957, 1958]. These observations were made at 38, 81 and 158 MHz over baselines ranging from 60 - 1000 meters. Crab nebula occultation observations at 26.3 and 38 MHz over the baselines of $\approx$ 700 - 1630 meters were made during 1961 and 1962 by *Hewish and Wyndham* [1963]. Furthermore, the normalized visibilities from the earlier observations, which were observed over different baselines and frequencies, are used after scaling them to 80 MHz and a baseline of 1.6 km using the general structure function discussed in § 3.2.

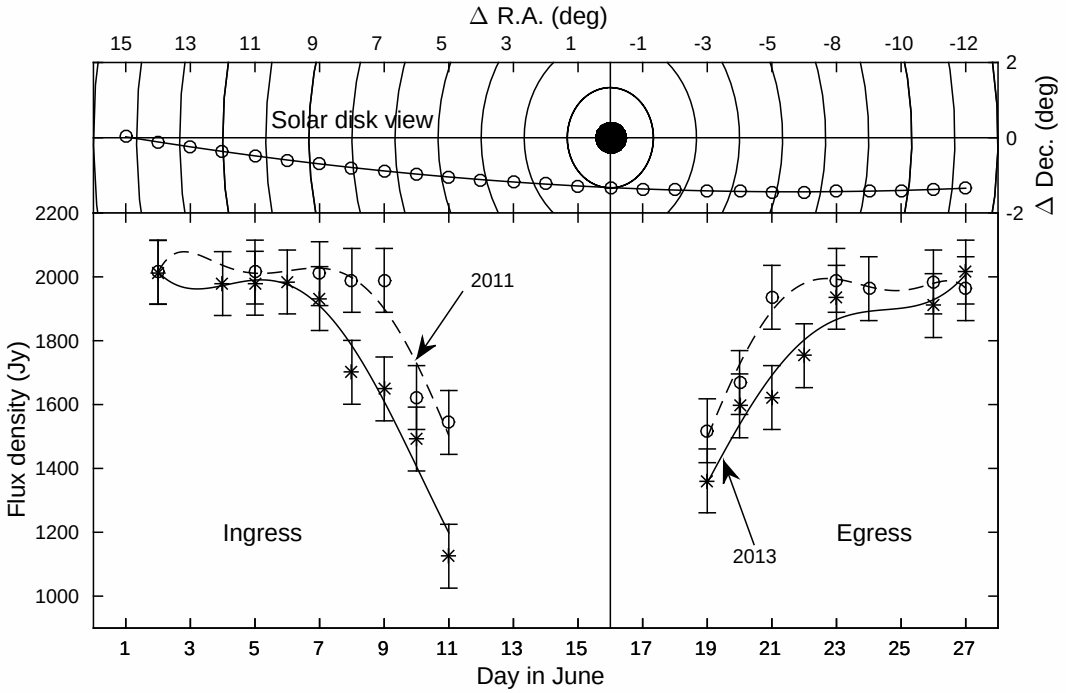

Figure 2. The upper panel shows solar disk view of the Crab nebula occultation. The filled circle indicates the Sun and open circles represent the position of Crab nebula with respect to the Sun on different dates; Δ R.A. and Δ Dec are the offset distances of Crab nebula from the Sun in right ascension and declination respectively. The closest concentric circle around the Sun has a radius of $5\ R_\odot$ and the radii of the rest of the circles differ from their adjacent ones by $5\ R_\odot$. The bottom panel shows the observed flux densities of the Crab nebula on different days during its occultation by the solar corona. The periods before and after June 16th correspond to the ingress and egress, respectively. The plots marked 'o' and '*' correspond to measurements during June 2011 and June 2013, respectively.

The primary observational quantity inferred from the Crab nebula occultation technique is the visibility $V(s)$, which is essentially the correlation between the voltages recorded by a pair of antennas. The visibility is a function of the observing baseline s. We will work with a quantity called the normalized visibility defined as $\Gamma(s) = V(s)/V(0)$. The structure function $D_\phi(s)$ which characterizes the phase perturbations caused by the density inhomogeneities in the medium is defined as [*Prokhorov et al.*, 1975; *Ishimaru*, 1978; *Coles and Harmon*, 1989; *Armstrong et al.*, 1990]

$$\Gamma(s) = e^{-D_\phi(s)/2}\,. \tag{5}$$

In other words,

$$D_\phi(s) = -2ln\Gamma(s) = -2ln\left[V(s)/V(0)\right]\,, \tag{6}$$

where $V(s)$ and $V(0)$ are the ensemble averaged values. For our purposes, $V(0)$ is the flux density of the Crab nebula when it was far from the Sun. Crab occultation observations are typically made using a single baseline; i.e., one value of s.

3.2 The General Structure Function (GSF)

Over the years, theoretical developments and observations have converged on a well accepted formulation for the structure function to describe density fluctuations in the solar wind (e.g., *Coles et al.* [1987]; *Armstrong et al.* [2000]; *Bastian* [1994]; *Subramanian and Cairns* [2011]). These expressions for the structure function, however, are valid only for situations where the baseline s is $\ll$ the inner scale $l_i(R)$ or is $\gg$ the inner scale. These approximations might not hold in our situation; for (depending upon the inner scale model one assumes) there are situations where the observing baseline s might be comparable to the inner scale. If this is the case, using the asymptotic expressions for the structure function will yield inaccurate results, and it is necessary to use the General Structure Function (GSF) that is valid for the asymptotic regimes $s \ll l_i(R)$ and $s \gg l_i(R)$ and also straddles the intermediate regime $s \approx l_i(R)$ [*Ingale et al.,* 2014]. Scatter-broadened images of sources observed against the background of the solar wind are observed to be anisotropic only for heliocentric distances $\leq$ 5–6 $R_\odot$ [*Anantharamaiah et al.,* 1994; *Armstrong et al.,* 1990]. Since our observations are made for distances ranging from 10 to 45 $R_\odot$, it is adequate to use the isotropic GSF, which is defined as follows:

$$\begin{aligned} D_\phi(s) \quad &= \tfrac{8\pi^2 r_e^2 \lambda^2 \Delta L}{2^{\alpha-2}(\alpha-2)} \Gamma\left(1-\tfrac{\alpha-2}{2}\right) \tfrac{C_N^2(R) l_i(R)^{\alpha-2}}{(1-f_p^2(R)/f^2)} \\ &\times \left\{ {}_1F_1\left[-\tfrac{\alpha-2}{2},\ 1,\ -\left(\tfrac{s}{l_i(R)}\right)^2 \right] - 1 \right\}, \end{aligned} \tag{7}$$

where ${}_1F_1$ is the confluent hypergeometric function, r_e is the classical electron radius, λ is the observing wavelength, R is the heliocentric distance, ΔL is the thickness of the scattering medium, f_p and f are the plasma and observing frequencies respectively. The functional form of the structure function is thus well known; the visibilities from the Crab occultation observations will provide one point that constrains its amplitude. The functional form of the structure function depends explicitly on the observing wavelength and the baseline. We use this dependence to normalise visibilities from Crab occultation observations made at different observing frequencies and wavelengths and baselines to an observing frequency of 80 MHz and a baseline of 1.6 km.

The origin of the inner (dissipation) scale $l_i(R)$ is a subject of intense ongoing research. While some researchers identify the inner scale with the proton inertial length [*Coles and Harmon*, 1989; *Harmon*, 1989; *Yamauchi et al.*, 1998b; *Verma et al.*, 1996; *Leamon et al.*, 1999, 2000; *Smith et al.*, 2001; *Bruno and Trenchi*, 2014], some use the proton gyroradius for the inner scale [*Bale et al.*, 2005; *Sahraoui et al.*, 2013; *Bisoi et al.*, 2014a]. These inner scale prescriptions are widely used in the literature, and we outline them in the §3.3 for completeness. There are several instances where the baseline lengths for the observations we consider are comparable to the inner scale. As shown in §3.3, the baseline length used in the 2011 and 2013 observations ($s = 1600$ meters) is comparable to the proton gyroradius for the relevant heliocentric distance range (≈ 10 – $45 R_\odot$). However, if the proton inertial length prescription is used for the inner scale, the typical baseline lengths are far smaller than the inner scale. We use the GSF (Eq 7), which covers all these situations; it is accurate for $s \ll l_i(R)$ through $s \approx l_i(R)$ and extending to $s \gg l_i(R)$.

3.3 Inner scale models

In this section we evaluate the inner scales in the solar wind using two different physical prescriptions and compare it with a fiducial interferometric baseline of 1600 meters.

3.3.1 Proton inertial length

The mechanism of proton cyclotron damping by Alfvén waves is often invoked to account for the dissipation scale of solar wind turbulence. The inner scale predicted by this mechanism is the proton inertial length (d_i), [*Coles and Harmon*, 1989; *Harmon*, 1989; *Yamauchi et al.*, 1998b; *Verma et al.*, 1996; *Leamon et al.*, 1999, 2000; *Smith et al.*, 2001; *Chen et al.*, 2014; *Bruno and Trenchi*, 2014] which can be written as

$$d_i(R) = 228 \times N_e(R)^{-1/2} \ \ \mathrm{km}, \tag{8}$$

where $N_e(R)$ is the background plasma density at heliocentric distance R in cm^{-3}. In order to calculate the background solar wind density, we start with daily peak values of the solar wind density at 1 AU during June 2011 and 2013 are used which were obtained from the Low Resolution OMNI (LRO) data set [1]. For the rest of the years, the background solar wind den-

[1] http://omniweb.gsfc.nasa.gov/form/dx1.html

sity at different heliocentric distances R (here, in units of AU) is extrapolated sunwards using the scaling predicted by the density model of *Leblanc et al.* [1998]:

$$N(R) = 7.2\ R^{-2} + 1.95 \times 10^{-3}\ R^{-4} + 8.1 \times 10^{-7}\ R^{-6}\ \ \mathrm{cm}^{-3}. \tag{9}$$

Equation 9 assumes a density of 7.2 cm^{-3} at 1 AU. To derive the background density at a specified R, equation 9 is multiplied by N(1 AU)/7.2, where N(1 AU) denotes the peak value of the background density from the LRO data set. For the rest of the years the default Leblanc density model is used.

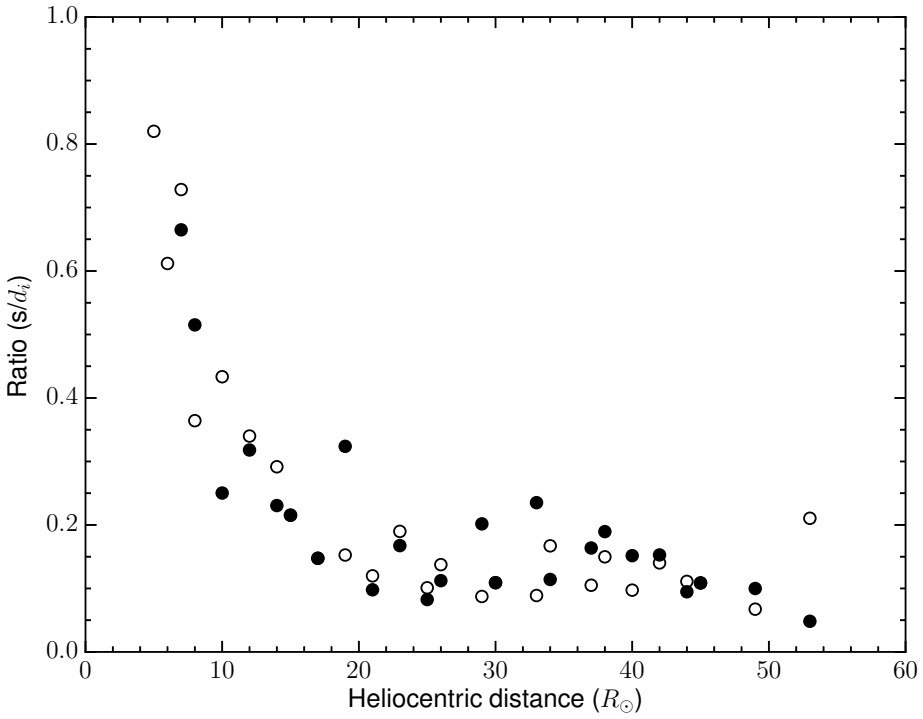

Figure 3. Scatter plot of the ratio of the baseline to proton inertial length (d_i) plotted against heliocentric distance. The open and filled circles denotes the data points derived using observations in June 2011 and 2013 respectively.

Figure 3 shows the ratio of the interferometric baseline used in June 2011 and 2013 (s = 1600 meters) to the proton inertial length. The open and filled circles correspond to the data points derived using observations in June 2011 and 2013 respectively. While s is comparable to the inner scale for $R < 10\ R_\odot$, it is significantly smaller than the inner scale for $R >$

$10\ R_\odot$. Since our data spans $45\ R_\odot > R > 10\ R_\odot$, it follows that the $s \ll l_i$ asymptotic branch is adequate if the inner scale is described by the proton inertial length.

3.3.2 Proton gyroradius

Another popular prescription for the inner/dissipation scale is the proton gyroradius [*Bale et al.,* 2005; *Sahraoui et al.,* 2013; *Bisoi et al.,* 2014a; *Chen et al.,* 2014]:

$$\rho_i(R) = 1.02 \times 10^2 \mu^{1/2} T_i^{1/2} B(R)^{-1} \ \ \mathrm{cm}, \tag{10}$$

where $\mu(\equiv m_i/m_p)$ is the mass of an ion, in units of the proton mass, T_i is the proton temperature in eV and B is the interplanetary magnetic field in Gauss. In order to estimate the magnetic field, we begin with the daily average interplanetary magnetic field (IMF) at 1 AU from the LRO data set during June 2011 and June 2013. In order to obtain the IMF at a given heliocentric distance R, we extrapolate these values Sunward using the Parker spiral magnetic field model in the ecliptic plane [*Williams,* 1995]:

$$B(R) = 3.4 \times 10^{-5} R^{-2} (1 + R^2)^{1/2} \ \ \mathrm{Gauss}, \tag{11}$$

where R is the heliocentric distance in units of AU. This equation assumes a magnetic field of $= 4.7{\times}10^{-5}$ Gauss at 1 AU. We multiply equation 11 with B(1 AU)/($4.7{\times}10^{-5}$), where B(1 AU) denotes the daily average IMF (in Gauss) obtained from the LRO data. Parker spiral magnetic field model is used as it is for the years other than 2011 and 2013. The inner scale lengths are calculated using equation 10 by assuming a proton temperatures of $T_i = 10^5$ K.

In the slow solar wind (300-400 km/s) the proton temperature would be $\approx 1 \times 10^5 - 6{\times}10^5$ K for heliocentric distances ranging from $\approx 0.2{-}0.05$ AU (i.e. $45{-}10\ R_\odot$). In the fast solar wind (700-800 km/s), the proton temperature would be $\approx 1.5{\times}10^6$ K at these heliocentric distances [*Marsch,* 1991]. The proton gyroradius for a proton temperature of $1.5{\times}$ 10^6K is $\approx 60\ \%$ larger than that for a proton temperature of 10^5K. We show the modulation index using a proton temperatures 10^5 K as well as 1.5×10^6 K in Figures 8 and 9.

Figure 4 shows the ratio of the interferometric baseline used for the June 2011 and 2013 observations (s = 1600 meters) to the proton gyroradius given by Eq 10. The open and filled circles denote the ratio corresponding to the observations in June 2011 and 2013 respectively for the proton temperatures $T_i = 10^5$ K. Evidently, $s \approx l_i(R)$ for 10–45 $R_\odot$, which is the

heliocentric distance range of interest to us. If the inner scale is the proton gyroradius, neither of the asymptotic approximations $s \ll l_i(R)$ or $s \gg l_i(R)$ is therefore appropriate, and the GSF needs to be used.

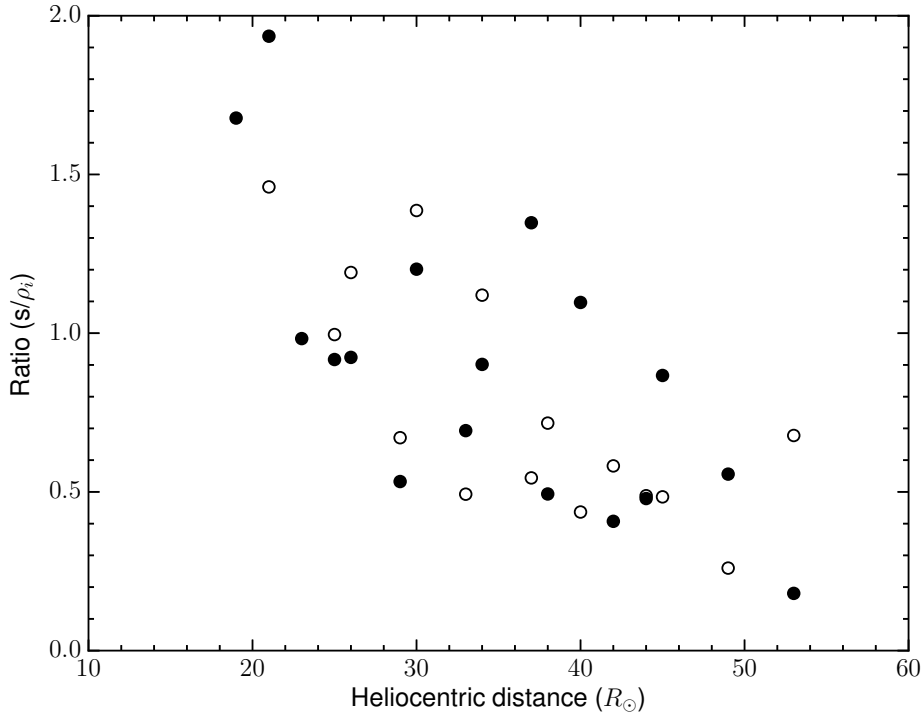

Figure 4. Scatter plot of the ratio of the baseline to proton gyroradius (ρ_i) plotted against heliocentric distance. The 'open' and 'filled' circles denote the data points derived using observations in June 2011 and 2013 respectively for the proton temperature $T_i = 10^5$ K.

3.4 Estimating the scattering measure

The scattering measure (SM) is defined as the path integral

$$\mathrm{SM} = \int C_N^2(R)\, dl \approx C_N^2(R)\, \Delta L\,, \tag{12}$$

where the integration is carried out over the depth over which scattering takes place. When the scattering is confined to a thin screen, the approximation indicated in Eq 12 is acceptable, where ΔL is the thickness of the scattering screen. We use the GSF defined in Eq 7 to calculate the scattering measure, which in turn will be used to determine $C_N^2(R)$. Accordingly,

$$\mathrm{SM} \quad = \quad C_N^2(R)\Delta L \tag{13}$$

$$= \left(f(\alpha,\lambda)\, \frac{l_i(R)^{\alpha-2}}{r_f(R,\lambda)}\, ({}_1F_1(\alpha,s,R)-1) \right)^{-1} D_\phi(s)$$

where,

$$\begin{aligned} f(\alpha,\lambda) &= \frac{8\pi^2 r_e^2 \lambda^2}{2^{\alpha-2}(\alpha-2)} \Gamma\left(1-\frac{\alpha-2}{2}\right), \\ r_f(R,\lambda) &= 1 - f_p^2(R)/f^2, \\ {}_1F_1(\alpha,s,R) &= {}_1F_1\left[-\frac{\alpha-2}{2}, 1, -\left(\frac{s}{l_i(R)}\right)^2\right], \end{aligned}$$

4 Results

4.1 Heliocentric dependence of C_N^2

As explained in §3, the structure function $D_\phi(s)$ can be computed from the basic observed quantity $V(s)$. In turn, the structure function can be used to calculate the scattering measure (Eq 13). We now describe how the SM can be used to estimate the turbulence amplitude $C_N^2(R)$ at different solar elongations R_0 (which correspond to different observation dates in June, and therefore to different heliocentric distances).

Assuming solar wind turbulence at these heliocentric distances ($10-45\ R_\odot$) to be spherically symmetric, the SM can also be expressed as [*Spangler and Sakurai*, 1995]:

$$\mathrm{SM} = \int_0^\infty C_N^2(R)\ \mathrm{d}R = \frac{\pi}{2} C_N^2(R_0)\, R_0 \tag{14}$$

$$C_N^2(R_0) = \frac{2}{\pi} \frac{\mathrm{SM}}{R_0} \tag{15}$$

where $C_N^2(R_0)$ denotes the amplitude of density turbulence at impact parameter R_0. The impact parameter R_0 is related to the solar elongation (see §52 in *Duffett-Smith and Zwart* [2011]) by a fraction $\approx 60/16$, where 16 is the solar radius in arc minute. Comparing with Eq 12 shows that the scattering screen thickness is identified as $\Delta L = (\pi/2)R_0$, in computing $C_N^2(R_0)$ from the scattering measure.

The SM is estimated from the observed structure function ($D_\phi(s)$) using two inner scale models: the proton inertial length and and proton gyroradius (see §3.3). We use a proton temperature of 10^5 K in the proton gyroradius prescription. Furthermore, the SM depends upon the assumed value of power law index (α) of the density fluctuation spectrum (Eq 1). Generally, the spectrum is observed to follow a Kolmogorov-like scaling with $\alpha = 11/3$. How-

ever, there is also some evidence for local flattening of the density fluctuation spectrum at large wave numbers [*Celnikier et al.*, 1987; *Coles and Harmon*, 1989; *Bastian*, 1994]; some authors therefore use $\alpha = 3$. In view of the lack of consensus on this issue, we compute the SM for $\alpha = 11/3$ as well as $\alpha = 3$. Subsequently, C_N^2 is calculated from the SM using Eq 15.

Using all the available data described in § 2, we compute C_N^2 as a function of heliocentric distance between 10 and 45 $R_\odot$. Since the observation span years corresponding to solar minimum as well as solar maximum, we have studied the data from each year separately. For instance, Figure 5 shows the variation of C_N^2 with heliocentric distance using data from 2013. We fit a function of the form $C_N^2(R) = A\ R^{-\gamma}$ to the data plotted in these Figures. We find that the data in Figure 5 suggests $A = 4 \times 10^5\ \mathrm{cm}^{-6}$ and $\gamma = -3.4$ with a goodness of fit (adjusted R^2) 0.72. Since we have a total of 44 such plots, we only show one representative example in Figure 5, and tabulate all our results in Table 4.2. It summarizes the heliocentric variation of C_N^2 for two values of α (11/3 and 3) and two inner scale models (the proton inertial length and the proton gyroradius). For instance, in 2011, $C_N^2(R) = 3.2{\times}10^4 R^{-2.8}$ for $\alpha = 3$ and the proton inertial length as the inner scale. On the other hand, $C_N^2(R) = 400R^{-2.1}$ for $\alpha = 3$ and the proton gyroradius (with proton temperature = 10^5 K) as the inner scale. Table 4.2 is thus a comprehensive representation of the heliocentric distance dependence of C_N^2 between 10 and 45 $R_\odot$. To the best of our knowledge, the only such result in the literature so far is due to *Spangler and Sakurai* [1995] and *Spangler et al.* [1996], who determined the heliocentric dependence of C_N^2 from 10 to 60 $R_\odot$ using VLBI observations during July and August 1991, which is $\approx$ 2 years past the maximum of cycle 22 in the declining phase. Their result, which assumes a Kolmogorov spectrum ($\alpha = 11/3$) is $C_N^2(R) = 3.81R^{-3.66}$ in units of $\mathrm{cm}^{-20/3}$; the same result is quoted in a slightly different form in Eq 2. Of the results we have compiled, data from 1960 corresponds to a similar phase in cycle 19. For this epoch, we obtain $C_N^2 \propto R^{-\gamma}$, with γ ranging from 3.2 to 3.3. Our results thus yield a remarkably similar dependence of C_N^2 with heliocentric distance for the only instance in the published literature where such a comparison can be made.

4.2 Solar cycle dependence of $C_N^2(R)$

It is evident from Table 4.2 that the values of A and γ are significantly different for different observation years, which correspond to different phases of the solar cycle. We investigate the solar cycle dependence of A and γ in Figures 6 and 7. The top and middle panels in the Figures 6 and 7 show the temporal variation of γ and A. For the comparison, the yearly

averaged sunspot number (SSN)[2] for different years are plotted in the bottom panel of Figures 6 and 7. Figure 6 corresponds to $\alpha = 3$ while Figure 7 refers to $\alpha = 11/3$. Upon comparing the top and middle panels with the bottom ones, it is evident that both A and γ are well correlated with the sunspot number. These trends hold irrespective of whether we use the proton gyroradius or proton inertial length prescription for the inner scale, and whether we use $\alpha = 11/3$ or $\alpha = 3$.

The correlation between A and the sunspot number is indicative of the fact that the overall magnitude of scattering is higher during solar maximum as compared to solar minimum. This is consistent with earlier results using interplanetary scattering observations [*Janardhan et al.*, 2011; *Manoharan*, 2012; *Janardhan et al.*, 2015].

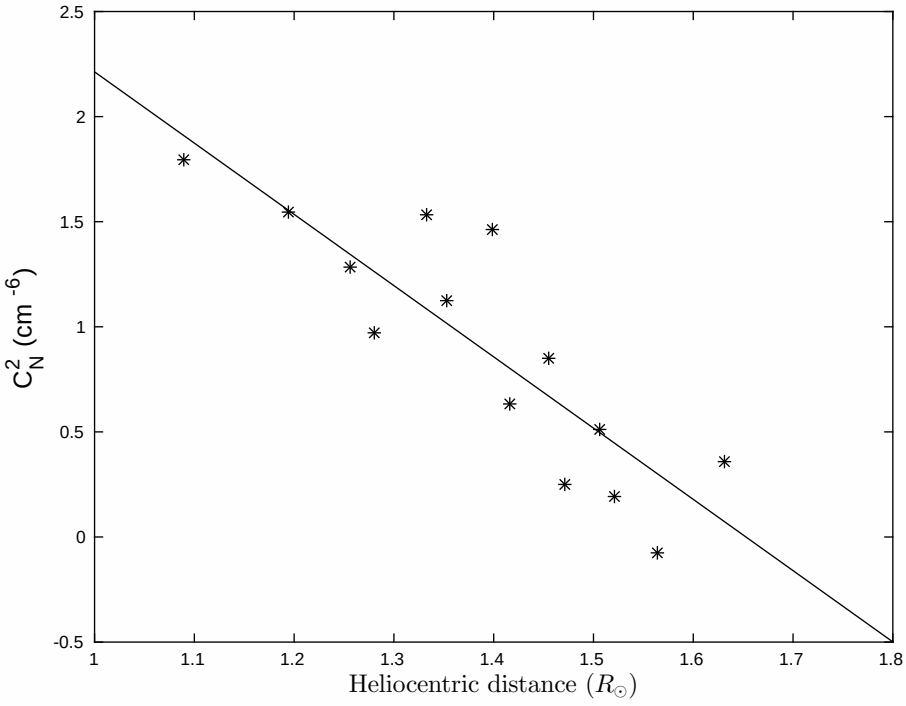

Figure 5. A log-log scatterplot of C_N^2 against heliocentric distance (in $R_\odot$) derived from observations in 2013. We use $\alpha = 3$ and the inner scale is the proton inertial length. The fit to $C_N^2(R) = A\,R^{-\gamma}$ yields $\gamma = 3.4$ and $A = 4 \times 10^5$ cm^{-6}.

The correlation between γ and the sunspot number indicates that the scattering strength falls off *faster* with heliocentric distance when solar activity increases. This might be because

[2] http://www.sidc.be/silso/datafiles

the large-scale solar magnetic field becomes more multipolar with increasing solar activity. For instance, this is reflected by the increasing complexity of the streamer belt with solar activity [*Wang et al.,* 2000; *Richardson and Kasper,* 2008]. Higher order multipolar fields are known to fall off more rapidly with heliocentric distance than a dipole, and this could be reflected in the spatial behaviour of the scattering strength, characterized by γ. Conversely, it has been reported earlier [*Tokumaru et al.,* 2000] that the scintillation index for IPS observations shows a rather shallow variation with heliocentric distance towards solar minimum. It should also be borne in mind that the Crab nebula passes from low latitudes to high(er) ones (upper panel of Figure 2). Near solar minimum, this means that it progresses from sampling the slow solar wind to the fast solar wind, and this is an additional complicating factor. Near solar maximum, the solar wind is relatively more symmetric with latitude, and is predominantly slow [*McComas et al.,* 2000; *Asai et al.,* 1998].

4.3 Heliocentric and solar cycle dependence of $\epsilon_N \equiv \delta N_{k_i}/N$

We next use our knowledge of C_N^2 to estimate the density modulation index ϵ_N using Eqs (3) and (4). We use *Leblanc et al.* [1998] prescription to evaluate the background solar wind density N. The heliocentric distance dependence of ϵ_N is shown in Figure 8 for different years. This quantity is computed using both the proton inertial length and proton gyroradius inner scale models. The broad conclusion that can be drawn from Figure 8 is that ϵ_N ranges between 0.001 and 0.1, and its only weakly dependent on heliocentric distance. The most we could discern was a linear dependence of ϵ_N with heliocentric distance with a slope of $1.45\times 10^{-3}\,R_\odot^{-1}$ in 1952. During solar maximum years, however, the slope was close to zero. We note that *Asai et al.* [1998] have investigated the solar wind speed dependence of the density modulation index usig IPS observations; this, in turn, can be related to solar cycle dependence.

Since the heliocentric distance dependence of ϵ_N is rather weak, it is meaningful to compute an average for this quantity for each year. The average of ϵ_N between 10 and 45 $R_\odot$ is plotted as a function of time in the upper panel of Figure 9. Comparison with the lower panel, which shows the sunspot numbers, shows that ϵ_N broadly follows the solar cycle.

However, we note that ϵ_N shows a prominent dip around 1958, which happens to be the year with the highest sunspot number of the data we have examined. Although the dip com-

S.No	Yearly averaged sunspot number	Observed Year	Proton inertial length				Proton gyroradius ($Ti = 10^5$ K)			
			$\alpha = 3$		$\alpha = 11/3$		$\alpha = 3$		$\alpha = 11/3$	
			γ	A (cm^{-6})	γ	A $(cm^{-20/3})$	γ	A (cm^{-6})	γ	A $(cm^{-20/3})$
1	261.7	1958	-4.2	8.6E+6	-4.9	3.6E+3	-3.7	2.1E+5	-4.7	1.1E+3
2	200.7	1956	-4.9	1.2E+8	-5.6	5.3E+4	-4.4	2.3E+6	-5.4	1.4E+4
3	159	1960	-2.7	8.1E+4	-3.3	3.3E+1	-2.3	3.7E+3	-3.2	1.2E+1
4	94	2013	-3.4	4.0E+5	-3.7	5.6E+1	-2.7	7.0E+3	-3.9	4.0E+1
5	80.8	2011	-2.8	3.2E+4	-3.2	4.9E+0	-2.1	4.0E+2	-3.0	1.2E+0
6	76.4	1961	-2.8	1.1E+5	-3.5	4.3E+1	-2.6	7.2E+3	-3.4	1.8E+1
7	54.2	1955	-4.9	4.0E+7	-5.6	1.8E+4	-4.2	5.2E+5	-5.3	4.2E+3
8	53.4	1962	-2.2	2.2E+3	-2.8	1.3E+0	-2.5	1.8E+3	-2.9	7.4E-1
9	45	1952	-2.1	3.7E+4	-2.7	1.1E+1	-1.7	1.4E+3	-2.6	5.3E+0
10	20.1	1953	-2.7	1.5E+5	-3.4	6.8E+1	-2.3	4.7E+3	-3.2	2.0E+1
11	6.6	1954	-2.9	1.4E+5	-3.6	6.4E+1	-2.8	1.1E+4	-3.6	2.7E+1

Table 1. C_N^2 as a function of heliocentric distance deduced from our observations. We fit the data for each year with a function of the form $C_N^2(R) = A\, R^{-\gamma}$. This Table shows values for A and γ.

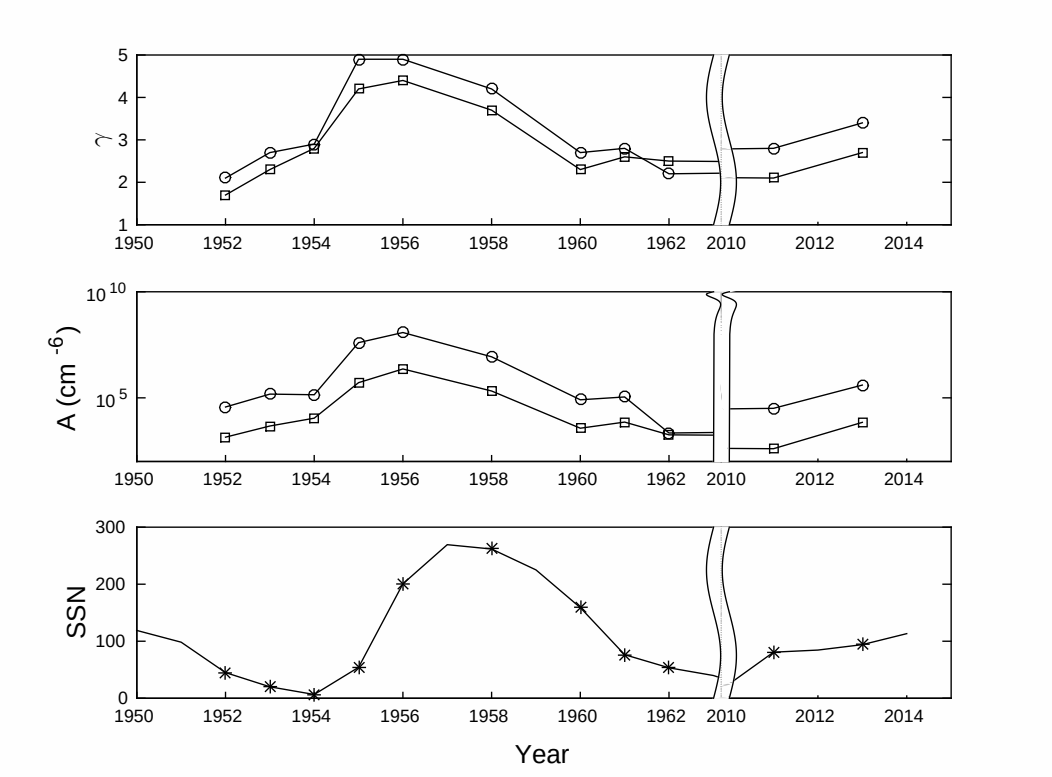

Figure 6. The top panel and middle panel show γ and A (cm^{-6}) respectively as a function of time. The 'circles' and 'squares' represent the proton inertial and proton gyroradius inner scale models respectively with $\alpha = 3$. For the proton gyroradius model, we use a temperature of 10^5 K. The solid line in the bottom panel shows the yearly averaged sunspot number and the '*' represents the year in which the Crab occultation measurements were made. It is evident that both γ and A correlate well with the solar cycle.

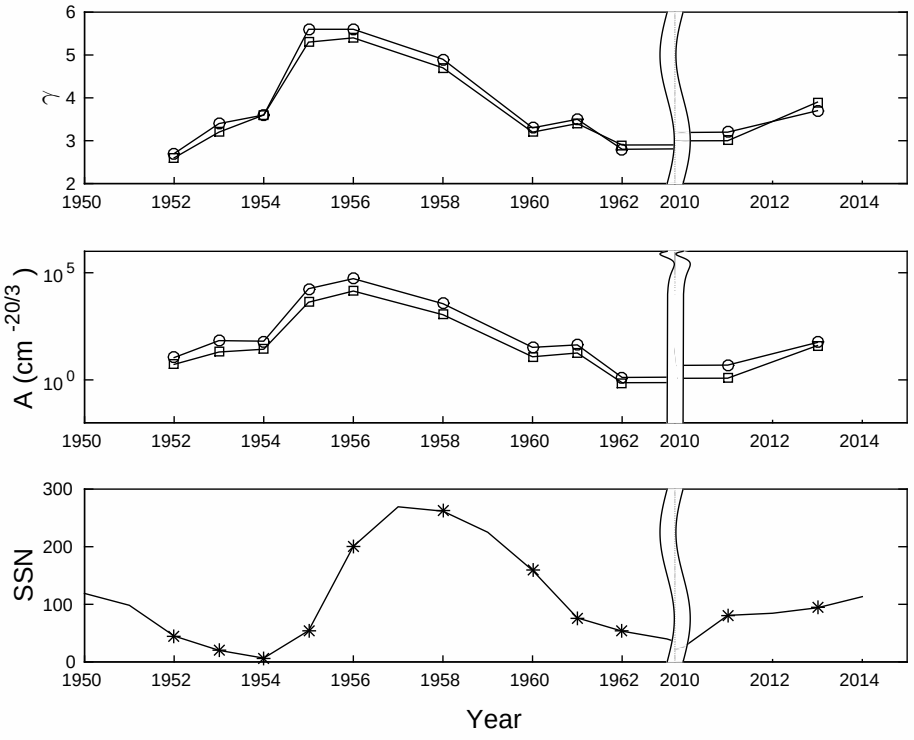

Figure 7. Same as Figure 6, except for α, which is 11/3. The dimensions of A are therefore $cm^{-20/3}$.

prises only one data point, the following could be a tentative explanation for it: *Celnikier et al.* [1987] notes that the modulation index (ϵ_N) is positively correlated with the temperature of solar wind protons. At 1 AU, it is also observed that the proton temperature is positively correlated with solar wind speed [*Lopez and Freeman*, 1986]. Taken together, this implies that ϵ_N should be larger in the fast solar wind than in the slow solar wind. During the solar minimum, the Sun's large-scale magnetic field is predominantly dipolar. Consequently, higher latitudes are dominated by fast ($\approx 700\ km/s$) solar wind emanating from coronal holes. Lower latitudes, on the other hand, are dominated by the slow solar wind ($\approx\ 400\ km/s$) emanating from near the streamer belt. During solar maximum, however, the large-scale solar magnetic fields is multi polar. Coronal holes are not as prevalent and slow solar wind is observed over all heliolatitudes [*McComas et al.*, 2000; *Asai et al.*, 1998]. Since 1958 was associated with a high sunspot number (the highest of the years we have considered), we expect slow solar wind (and low proton temperatures) at all heliolatitudes because the magnetic field is multipolar.

Furthermore, *Asai et al.* [1998] suggest that the modulation index of the high speed solar wind (which is usually observed near solar minimum) shows significant evolution with he-

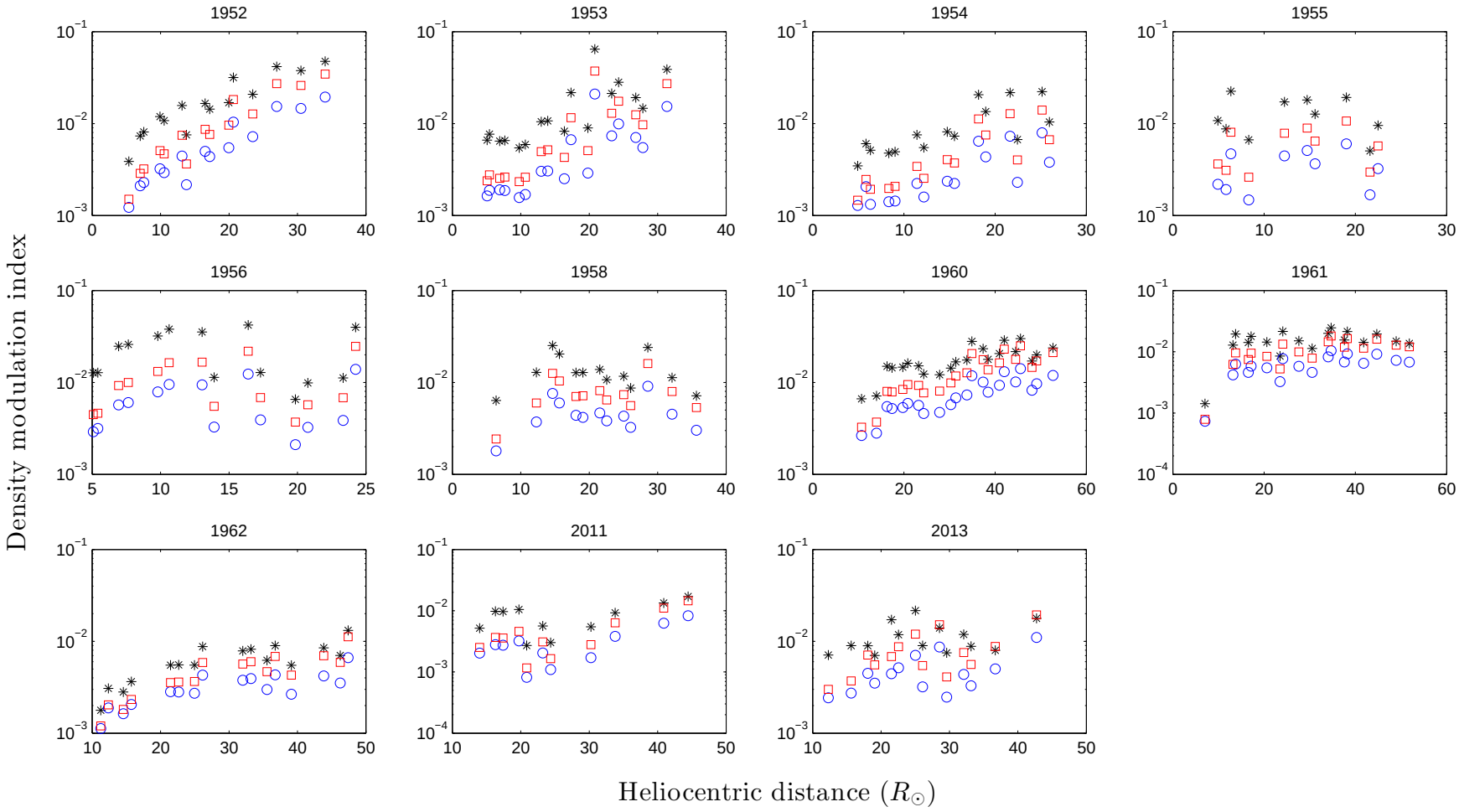

Figure 8. The Figure shows the measured density fluctuation index (ϵ_N) over a heliocentric distance in different years using different inner scale models. The '*' indicates the proton inertial length model and 'circles' and 'squares' represent the proton gyroradius model with proton temperature 10^5 and 1.5×10^6 K respectively.

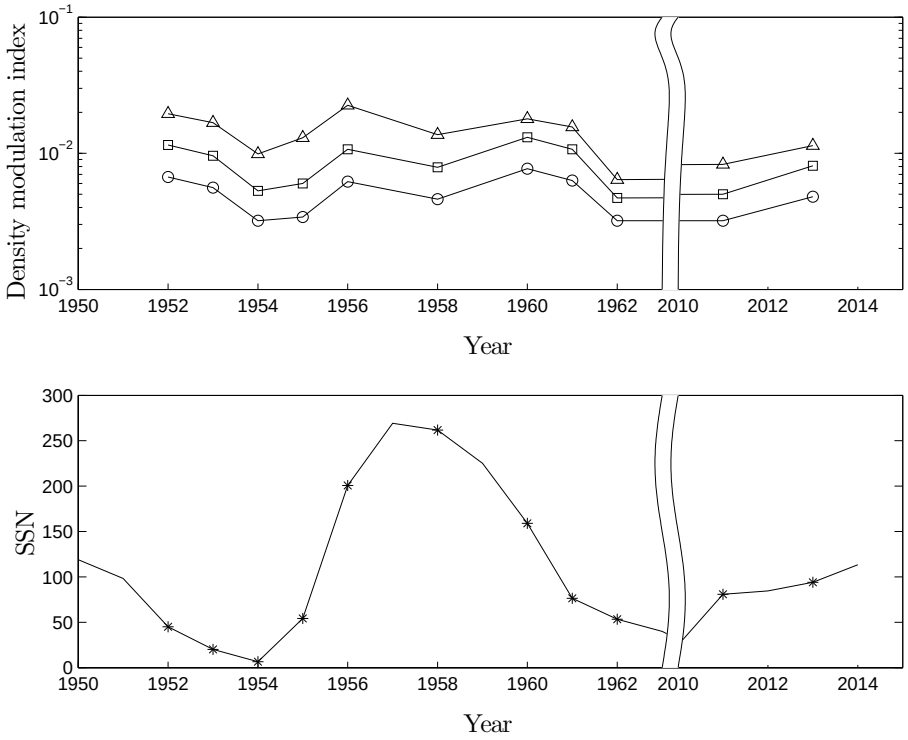

Figure 9. The top panel of the Figure shows variation of the density fluctuations in different years is an evidence of their dependence on solar cycle. The 'triangles' indicate the proton inertial length model and the 'circles' and 'squares' indicate the proton gyroradius model with the proton temperature 10^5 and 1.5×10^6 K respectively. In the lower panel, '*' indicates the average sunspot number on corresponding years.

liocentric distance. Our results (Figure 8) show that the modulation index does not vary appreciably with heliocentric distance during the solar maximum years of 1956, 1958, 1960, 1961 and 2013, when the slow solar wind is expected to dominate. Our results are thus consistent with the converse of the conclusions reached by *Asai et al.* [1998].

5 Summary and Conclusions

Density fluctuations are an important and relatively ill-understood facet of the phenomenon of solar wind turbulence. Most studies of solar wind turbulence in general, and density fluctuations in particular, concentrate on the spectral slope (α, Eq 1), and not so much on its spectral amplitude (C_N^2, Eq 1). Needless to say, the amplitude of the density turbulence spectrum is key to several important problems such as extended solar wind heating and angular broadening of radio sources. Our knowledge of C_N^2 (and its heliocentric dependence in particular) is currently limited to the investigations of *Spangler and Sakurai* [1995] and *Spangler et al.*

[1996] (quoted in Eq 2), who used VLBI observations made 2 years past the maximum of cycle 19 to probe scale sizes ≥ 200 km. Their formulation used the Kolmogorov scaling ($\alpha = 11/3$) and did not consider an inner/dissipation scale. The density modulation index ϵ_N (Eq 4) is somewhat better studied. However, most of these studies have rather sparse coverage, and the only comprehensive study of this quantity that we are aware of *Bisoi et al.* [2014a] is only for heliocentric distances $> 40R_\odot$.

We use results from the standard technique of Crab nebula occultation to obtain a comprehensive palette of results concerning the heliocentric dependence of the density turbulence spectral amplitude (C_N^2) and the density modulation index (ϵ_N) for $10 < R < 45R_\odot$. This is a distance range that is typically not covered by either IPS or interferometric techniques. We include the effects of the inner scale using currently prevalent models for it. Since the spatial scales used are small enough to possibly be comparable to the inner/dissipation scale, we use the general structure function (GSF) to model the observed visibilities rather than asymptotic approximations. Since there is evidence for flattening of the spectrum near the inner scale, we quote results for $\alpha = 11/3$ as well as a flatter value of 3. We parametrize the heliocentric dependence of the density turbulence amplitude as $C_N^2(R) = A\,R^{-\gamma}$; the values of A and γ from our observations are shown in Table 4.2. This gives an idea of the range of possibilities for the behavior of C_N^2 using currently prevalent ideas. To the best of our knowledge, this is the most extensive characterization of the density turbulence spectral amplitude to date. For example, for the proton inertial length prescription for the inner scale and $\alpha = 3$, 'A' ranges from 2.2×10^3 to 1.2×10^8 cm^{-6} and γ ranges from -2.1 to -4.9. With the same inner scale prescription, with $\alpha = 11/3$, 'A' varies between 1.3 and $5.3{\times}10^4$ $m^{-20/3}$ and γ ranges from -2.7 to -5.6. With the proton gyroradius inner scale model and $\alpha = 3$, 'A' ranges from $4{\times}10^2 - 2.3{\times}10^6$ cm^{-6} and γ ranges from -1.7 to -4.4. With the proton gyroradius inner scale model and $\alpha = 11/3$, 'A' ranges from 0.74 to $1.4{\times}10^4$ $cm^{-20/3}$ and γ varies from -2.6 to -5.4. In the only instance where our results can be compared with the existing results of *Spangler and Sakurai* [1995] and *Spangler et al.* [1996], our values for γ agree well with theirs. Given the widely different observational and theoretical interpretation techniques we use, and the fact that the observations we are using for comparison are from a different solar cycle, this is remarkable.

Since we have used data from varying stages of the solar cycle, we investigate the solar cycle dependence of A and γ; the results for which are summarized in Figures 6 and 7. The behavior of A confirms the well known fact that the overall strength of scattering increases

with increasing solar activity and vice-versa. Our results for γ imply that the scattering amplitude decreases more rapidly with heliocentric distance with increasing solar activity. This is intriguing, and could reflect the increasingly multipolar nature of the large-scale coronal magnetic field near solar maximum, since higher order multipoles decay more rapidly with distance. Taken together, our results could have interesting implications for the connection between density fluctuations and the large scale solar magnetic field. The possible connection between declining (large-scale) polar fields and the density turbulence levels probed by the IPS technique has been pointed out earlier [*Janardhan et al.,* 2010, 2011, 2015; *Bisoi et al.,* 2014b]. Our results are an interesting complementary take on this problem, using a different technique and for heliocentric distances that are much closer to the Sun.

We also use our knowledge of C_N^2 to obtain the density modulation index as defined in Eqs (3) and (4). In agreement with the results of *Bisoi et al.* [2014a] for larger heliocentric distances, we find that ϵ_N depends only weakly on heliocentric distance. While *Bisoi et al.* [2014a] found that ϵ_N shows a monotonic decline of around 8 % over solar cycle 23, we find that ϵ_N closely tracks the solar cycle, with a peak-to-peak variation (from 1956 to 1962) of around 72 %. Our results on the density modulation index can be used to investigate some important questions regarding the solar wind: it can be used to calculate the extended solar wind heating rate, and it provides yet another way of investigating the relation between density turbulence, the large scale magnetic field and turbulent magnetic field fluctuations.

Acknowledgments

- The Crab nebula occultation data for 2011 and 2013 is available on request from the Gauribidanur observatory, operated by Indian Institute of Astrophysics, Bangalore, India. Email-id: ramesh@iiap.res.in.
- PS acknowledges support from the ISRO-RESPOND program.
- The authors would like to thank the anonymous referees for their valuable and constructive suggestions.

References

Anantharamaiah, K. R., P. Gothoskar, and T. J. Cornwell (1994), Radio Synthesis Imaging of Anisotropic Angular Broadening in the Solar Wind, *J. Astrophys. Astron., 15*, 387.

Armstrong, J. W., W. A. Coles, B. J. Rickett, and M. Kojima (1990), Observations of

field-aligned density fluctuations in the inner solar wind, *The Astrophysical Journal*, *358*, 685–692, doi:10.1086/169022.

Armstrong, J. W., W. A. Coles, and B. J. Rickett (2000), Radio wave scattering in the outer heliosphere, *Journal of Geophysical Research (Space Physics)*, *105*, 5149–5156, doi:10.1029/1999JA900471.

Asai, K., M. Kojima, M. Tokumaru, A. Yokobe, B. V. Jackson, P. L. Hick, and P. K. Manoharan (1998), Heliospheric tomography using interplanetary scintillation observations. III - Correlation between speed and electron density fluctuations in the solar wind, *Journal of Geophysical Research (Space Physics)*, *103*, 1991, doi: 10.1029/97JA02750.

Bale, S. D., P. J. Kellogg, F. S. Mozer, T. S. Horbury, and H. Reme (2005), Measurement of the Electric Fluctuation Spectrum of Magnetohydrodynamic Turbulence, *Physical Review Letters*, *94*(21), 215002, doi:10.1103/PhysRevLett.94.215002.

Bastian, T. S. (1994), Angular scattering of solar radio emission by coronal turbulence, *The Astrophysical Journal*, *426*, 774–781, doi:10.1086/174114.

Bastian, T. S. (2004), Low-frequency solar radiophysics with LOFAR and FASR, *Planet. Space Sci.*, *52*, 1381.

Bavassano, B., and R. Bruno (1995), Density fluctuations and turbulent Mach numbers in the inner solar wind, *Journal of Geophysical Research (Space Physics)*, *100*, 9475–9480, doi:10.1029/94JA03048.

Bisi, M. M., B. V. Jackson, A. Buffington, J. M. Clover, P. P. Hick, and M. Tokumaru (2009), Low-Resolution STELab IPS 3D Reconstructions of the Whole Heliosphere Interval and Comparison with in-Ecliptic Solar Wind Measurements from STEREO and Wind Instrumentation, *Solar Physics*, *256*, 201–217, doi:10.1007/s11207-009-9350-9.

Bisi, M. M., B. V. Jackson, A. R. Breen, G. D. Dorrian, R. A. Fallows, J. M. Clover, and P. P. Hick (2010), Three-Dimensional (3-D) Reconstructions of EISCAT IPS Velocity Data in the Declining Phase of Solar Cycle 23, *Solar Physics*, *265*, 233–244, doi:10.1007/s11207-010-9594-4.

Bisoi, S. K., P. Janardhan, M. Ingale, P. Subramanian, S. Ananthakrishnan, M. Tokumaru, and K. Fujiki (2014a), A Study of Density Modulation Index in the Inner Heliospheric Solar Wind during Solar Cycle 23, *The Astrophysical Journal*, *795*, 69.

Bisoi, S. K., P. Janardhan, D. Chakrabarty, S. Ananthakrishnan, and A. Divekar (2014b), Changes in Quasi-periodic Variations of Solar Photospheric Fields: Precursor to the

Deep Solar Minimum in Cycle 23?, *Solar Physics*, *289*, 41–61, doi:10.1007/s11207-013-0335-3.

Bruno, R., and L. Trenchi (2014), Radial Dependence of the Frequency Break between Fluid and Kinetic Scales in the Solar Wind Fluctuations, *The Astrophysical Journal Letters*, *787*, L24, doi:10.1088/2041-8205/787/2/L24.

Cairns, I. H. (2004), Solar, interplanetary, planetary, and related extra-solar system science for LOFAR, *Planet. Space Sci.*, *52*, 1423.

Carbone, V., R. Marino, L. Sorriso-Valvo, A. Noullez, and R. Bruno (2009), Scaling Laws of Turbulence and Heating of Fast Solar Wind: The Role of Density Fluctuations, *Physical Review Letters*, *103*(6), 061102, doi:10.1103/PhysRevLett.103.061102.

Celnikier, L. M., L. Muschietti, and M. V. Goldman (1987), Aspects of interplanetary plasma turbulence, *Astronomy & Astrophysics*, *181*, 138–154.

Chandran, B. D. G., E. Quataert, G. G. Howes, Q. Xia, and P. Pongkitiwanichakul (2009), Constraining Low-Frequency Alfvénic Turbulence in the Solar Wind Using Density-Fluctuation Measurements, *The Astrophysical Journal*, *707*, 1668–1675, doi:10.1088/0004-637X/707/2/1668.

Chen, C. H. K., L. Leung, S. Boldyrev, B. A. Maruca, and S. D. Bale (2014), Ion-scale spectral break of solar wind turbulence at high and low beta, *Geophysical Research Letters*, *41*, 8081–8088, doi:10.1002/2014GL062009.

Cohen, M. H., and E. J. Gundermann (1969), Interplanetary Scintillations.IV. Observations Near the Sun, *The Astrophysical Journal*, *155*, 645, doi:10.1086/149897.

Coles, W. A., and J. K. Harmon (1989), Propagation observations of the solar wind near the sun, *The Astrophysical Journal*, *337*, 1023–1034, doi:10.1086/167173.

Coles, W. A., B. J. Rickett, J. L. Codona, and R. G. Frehlich (1987), Refractive scintillation in the interstellar medium, *The Astrophysical Journal*, *315*, 666–674, doi:10.1086/165168.

Coles, W. A., W. Liu, J. K. Harmon, and M. C. L. (1991), The solar wind density spectrum near the sun - Results from Voyager radio measurements, *Journal of Geophysical Research (Space Physics)*, *96*, 1745–1755.

Duffett-Smith, P., and J. Zwart (2011), *Practical Astronomy with your Calculator or Spreadsheet*.

Ekers, R. D., and L. T. Little (1971), The Motion of the Solar Wind Close to the Sun, *Astronomy & Astrophysics*, *10*, 310.

Erickson, W. C. (1964), The Radio-Wave Scattering Properties of the Solar Corona., *The Astrophysical Journal*, *139*, 1290, doi:10.1086/147865.

Harmon, J. K. (1989), Compressibility and cyclotron damping in the oblique Alfven waves, *Journal of Geophysical Research (Space Physics)*, *94*, 15,399–15,405, doi: 10.1029/JA094iA11p15399.

Hewish, A. (1957), Occultation of the Crab nebula by the solar corona, *The Observatory*, *77*, 151–153.

Hewish, A. (1958), The scattering of radio waves in the solar corona, *Monthly Notices of the Royal Astronomical Society*, *118*, 534, doi:10.1093/mnras/118.6.534.

Hewish, A., and J. D. Wyndham (1963), The solar corona in the interplanetary space, *Monthly Notices of the Royal Astronomical Society*, *126*, 469.

Hewish, A., P. F. Scott, and D. Wills (1964), Interplanetary Scintillation of Small Diameter Radio Sources, *Nature*, *203*, 1214–1217, doi:10.1038/2031214a0.

Hnat, B., S. C. Chapman, and G. Rowlands (2005), Compressibility in Solar Wind Plasma Turbulence, *Physical Review Letters*, *94*(20), 204502, doi: 10.1103/PhysRevLett.94.204502.

Imamura, T., M. Tokumaru, H. Isobe, D. Shiota, H. Ando, M. Miyamoto, T. Toda, B. Häusler, M. Pätzold, A. Nabatov, A. Asai, K. Yaji, M. Yamada, and M. Nakamura (2014), Outflow Structure of the Quiet Sun Corona Probed by Spacecraft Radio Scintillations in Strong Scattering, *The Astrophysical Journal*, *788*, 117, doi:10.1088/0004-637X/788/2/117.

Ingale, M., P. Subramanian, and I. H. Cairns (2014), Coronal turbulence and the angular broadening of radio sources - the role of the structure function, *Monthly Notices of the Royal Astronomical Society*, *447*, 34,861.

Ishimaru, A. (1978), *Wave propagation and scattering in random media, Vol.1 (New York: Academic Press)*.

Janardhan, P., and S. K. Alurkar (1993), Angular source size measurements and interstellar scattering at 103 MHz using interplanetary scintillation, *Astronomy & Astrophysics*, *269*, 119–127.

Janardhan, P., S. K. Bisoi, and S. Gosain (2010), Solar Polar Fields During Cycles 21 - 23: Correlation with Meridional Flows, *Solar Physics*, *267*, 267–277, doi: 10.1007/s11207-010-9653-x.

Janardhan, P., S. K. Bisoi, S. Ananthakrishnan, M. Tokumaru, and K. Fujiki (2011), The

prelude to the deep minimum between solar cycles 23 and 24: Interplanetary scintillation signatures in the inner heliosphere, *Geophysical Research Letters*, *38*, L20108, doi:10.1029/2011GL049227.

Janardhan, P., S. K. Bisoi, S. Ananthakrishnan, M. Tokumaru, K. Fujiki, L. Jose, and R. Sridharan (2015), A 20 year decline in solar photospheric magnetic fields: Inner-heliospheric signatures and possible implications, *Journal of Geophysical Research (Space Physics)*, *120*, 5306–5317, doi:10.1002/2015JA021123.

Kathiravan, C., R. Ramesh, Indrajit V. Barve, and R. M. (2011), Radio Observations of the Solar Corona During an Eclipse, *The Astrophysical Journal*, *730*, 91.

Kerdraon, A. (1979), Observation of small size solar radio bursts at metric wavelengths, *Astronomy & Astrophysics*, *71*, 266.

Kundu, M. R. (1965), *Solar Radio Astronomy (New York: John Wiley & Sons, Inc.), 600*.

Lang, K. R., and R. F. Willson (1987), VLA observations of a solar noise storm, *The Astrophysical Journal*, *319*, 514.

Leamon, R. J., C. W. Smith, N. F. Ness, and H. K. Wong (1999), Dissipation range dynamics: Kinetic Alfvén waves and the importance of <formula alphabet="latin">$\beta_{<italic>e</italic>}$, *Journal of Geophysical Research (Space Physics)*, *104*, 22,331–22,344, doi:10.1029/1999JA900158.

Leamon, R. J., W. H. Matthaeus, C. W. Smith, G. P. Zank, D. J. Mullan, and S. Oughton (2000), MHD-driven Kinetic Dissipation in the Solar Wind and Corona, *The Astrophysical Journal*, *537*, 1054–1062, doi:10.1086/309059.

Leblanc, Y., G. A. Dulk, and J. L. Bougeret (1998), Tracing the Electron Density from the Corona to 1AU, *Solar Physics*, *183*, 165.

Lopez, R. E., and J. W. Freeman (1986), Solar wind proton temperature-velocity relationship, *Journal of Geophysical Research (Space Physics)*, *91*, 1701–1705, doi:10.1029/JA091iA02p01701.

Machin, K. E., and F. G. Smith (1952), Occultation of a Radio Star by the Solar Corona, *Nature*, *170*, 319–320, doi:10.1038/170319b0.

Manoharan, P. K. (1993), Three-dimensional structure of the solar wind: Variation of density with the solar cycle, *Solar Physics*, *148*, 153.

Manoharan, P. K. (2012), Three-dimensional Evolution of Solar Wind during Solar Cycles 22-24, *The Astrophysical Journal*, *751*, 128, doi:10.1088/0004-637X/751/2/128.

Manoharan, P. K., M. Kojima, N. Gopalswamy, T. Kondo, and Z. Smith (2000), Radial

Evolution and Turbulence Characteristics of a Coronal Mass Ejection, *The Astrophysical Journal*, *530*, 1061–1070, doi:10.1086/308378.

Marsch, E. (1991), *Kinetic Physics of the Solar Wind Plasma*, p. 152.

Marsch, E., and C.-Y. Tu (1990), Spectral and spatial evolution of compressible turbulence in the inner solar wind, *Journal of Geophysical Research (Space Physics)*, *95*, 11,945–11,956, doi:10.1029/JA095iA08p11945.

McComas, D. J., B. L. Barraclough, H. O. Funsten, J. T. Gosling, E. Santiago-Muñoz, R. M. Skoug, B. E. Goldstein, M. Neugebauer, P. Riley, and A. Balogh (2000), Solar wind observations over Ulysses' first full polar orbit, *Journal of Geophysical Research (Space Physics)*, *105*, 10,419–10,434, doi:10.1029/1999JA000383.

Mercier, C., P. Subramanian, A. Kerdraon, M. Pick, S. Ananthakrishnan, and P. Janardhan (2006), Combining visibilities from the giant meterwave radio telescope and the Nancay radio heliograph. High dynamic range snapshot images of the solar corona at 327 MHz, *Astronomy & Astrophysics*, *447*, 1189.

Mercier, C., P. Subramanian, G. Chambe, and P. Janardhan (2015), The structure of solar radio noise storms, *Astronomy & Astrophysics*, *576*, A136, doi:10.1051/0004-6361/201321064.

Mugundhan, V., R. Ramesh, Indrajit V. Barve, C. Kathiravan, G. Gireesh, P. Kharb, and M. Apurva (2016), Low frequency radio observations of the solar corona with arcmin angular resolution: Implications for coronal turbulence and weak energy releases, *The Astrophysical Journal*, *831*, 154–160.

Prokhorov, A. M., F. V. Bunkin, K. S. Gochelashvili, and V. I. Shishov (1975), Laser irradiance propagation in turbulent media, *Proc. IEEE*, *63*, 790–811.

Ramesh, R. (2000a), Low Frequency Radio Emission from the 'Quiet Sun', *Journal of Astrophysics and Astronomy*, *21*, 237, doi:10.1007/BF02702398.

Ramesh, R. (2011), Low frequency solar radio astronomy at the Indian Institute of Astrophysics (IIA), *Bull. Astron. Soc. India Conf. Ser.*, *2*, 55.

Ramesh, R., and E. Ebenezer (2001), Decameter Wavelength Observations of an Absorption Burst from the Sun and Its Association with an X2.0/3B Flare and the Onset of a "Halo" Coronal Mass Ejection, *The Astrophysical Journal*, *558*, L141.

Ramesh, R., and C. V. Sastry (2000b), Radio observations of a coronal mass ejection induced depletion in the outer solar corona, *Astronomy & Astrophysics*, *358*, 749.

Ramesh, R., K. R. Subramanian, and C. V. Sastry (1999), Eclipse Observations of Com-

pact Sources in the Outer Solar Corona, *Solar Physics*, *185*, 77.

Ramesh, R., C. Kathiravan, and C. V. Sastry (2001), Low-Frequency Radio Observations of the Angular Broadening of the Crab Nebula Due to a Coronal Mass Ejection, *The Astrophysical Journal*, *548*, L229–L231, doi:10.1086/319098.

Ramesh, R., H. S. Nataraj, C. Kathiravan, and C. V. Sastry (2006), The Equatorial Background Solar Corona during Solar Minimum, *The Astrophysical Journal*, *648*, 707–711, doi:10.1086/505677.

Ramesh, R., C. Kathiravan, I. V. Barve, and M. Rajalingam (2012), High Angular Resolution Radio Observations of a Coronal Mass Ejection Source Region at Low Frequencies during a Solar Eclipse, *The Astrophysical Journal*, *744*, 165.

Reid, H. A. S., and E. P. Kontar (2010), Solar Wind Density Turbulence and Solar Flare Electron Transport from the Sun to the Earth, *The Astrophysical Journal*, *721*, 864–874, doi:10.1088/0004-637X/721/1/864.

Richardson, J. D., and J. C. Kasper (2008), Solar cycle variations of solar wind dynamics and structures, *Journal of Atmospheric and Solar-Terrestrial Physics*, *70*, 219–225, doi:10.1016/j.jastp.2007.08.039.

Rickett, B. J. (1990), Radio propagation through the turbulent interstellar plasma, *Annual Review of Astronomy & Astrophysics*, *28*, 561.

Riddle, A. C. (1974), On the Observation of Scattered Radio Emission from Sources in the Solar Corona, *Solar Physics*, *35*, 153.

Sahraoui, F., S. Y. Huang, G. Belmont, M. L. Goldstein, A. Rétino, P. Robert, and J. De Patoul (2013), Scaling of the Electron Dissipation Range of Solar Wind Turbulence, *The Astrophysical Journal*, *777*, 15, doi:10.1088/0004-637X/777/1/15.

Sakurai, T. (1993), Radioastronomical measurements of plasma characteristics of the solar corona and the solar wind, Ph.D. thesis, Iowa Univ., Iowa City, IA.

Sastry, C. V. (1994), Observations of the continuum radio emission from the undisturbed Sun at a wavelength of 8.7 meters, *Solar Physics*, *150*, 285–294, doi: 10.1007/BF00712890.

Sastry, C. V., and K. R. Subramanian (1974), Observations on the occultation of the radio source Tauras A by the solar corona during June 1971, *Ind. J. Radio and Space Phys.*, *3*, 196–198.

Smith, C. W., D. J. Mullan, N. F. Ness, R. M. Skoug, and J. Steinberg (2001), Day the solar wind almost disappeared: Magnetic field fluctuations, wave refraction and dis-

sipation, *Journal of Geophysical Research (Space Physics)*, *106*, 18,625–18,634, doi: 10.1029/2001JA000022.

Spangler, S. R. (2002), The Amplitude of Magnetohydrodynamic Turbulence in the Inner Solar Wind, *The Astrophysical Journal*, *576*, 997–1004, doi:10.1086/341889.

Spangler, S. R., and T. Sakurai (1995), Radio interferometer observations of solar wind turbulence from the orbit of HELIOS to the solar corona, *The Astrophysical Journal*, *445*, 999–1016, doi:10.1086/175758.

Spangler, S. R., T. Sakurai, W. A. Coles, R. R. Grall, and J. K. Harmon (1996), Radio interferometer observations of turbulence in the inner solar wind in Proc. of the Eighth International Solar Wind Conference, ed. Winterhatter, D., Gosling, J. T., Habbal, S. R., Kurth, W. S. and Neugebauer, M. (AIP Conf. Proc.) 382, 265, *Proc. of the Eighth International Solar Wind Conference, ed. Winterhatter, D., Gosling, J. T., Habbal, S. R., Kurth, W. S. and Neugebauer, M. (AIP Conf. Proc.), 382, 265*, *382*, 265.

Subramanian, K. R. (2004), Brightness temperature and size of the quiet Sun at 34.5 MHz, *Astronomy & Astrophysics*, *426*, 329–331, doi:10.1051/0004-6361:20047120.

Subramanian, P., and I. Cairns (2011), Constraints on coronal turbulence models from source sizes of noise storms at 327 MHz, *Journal of Geophysical Research (Space Physics)*, *116*, A03104, doi:10.1029/2010JA015864.

Thejappa, G., and M. R. Kundu (1992), Unusually low coronal radio emission at the solar minimum, *Solar Physics*, *140*, 19–39, doi:10.1007/BF00148427.

Thejappa, G., and R. J. MacDowall (2008), Effects of Scattering on Radio Emission from the Quiet Sun at Low Frequencies, *The Astrophysical Journal*, *676*, 1338–1345, doi:10.1086/528835.

Tokumaru, M., M. Kojima, Y. Ishida, A. Yokobe, and T. Ohmi (2000), Large-Scale Structure of Solar Wind Turbulence Near Solar Activity Minimum, *Advances in Space Research*, *25*, 1943–1946, doi:10.1016/S0273-1177(99)00630-4.

Tokumaru, M., M. Kojima, and K. Fujiki (2012), Long-term evolution in the global distribution of solar wind speed and density fluctuations during 1997-2009, *Journal of Geophysical Research (Space Physics)*, *117*, A06108, doi:10.1029/2011JA017379.

Tokumaru, M., K. Fujiki, M. Kojima, T. Iju, H. Nakano, D. Satonaka, T. Shimoyama, and K. Hakamada (2016), Global distribution of the solar wind and its evolution during cycles 22-24, *AIP Conference Proceedings*, *1720*(1), 030004, doi: http://dx.doi.org/10.1063/1.4943827.

Tu, C.-Y., and E. Marsch (1994), On the nature of compressive fluctuations in the solar wind, *Journal of Geophysical Research (Space Physics)*, *99*, 21, doi:10.1029/94JA00843.

Verma, M. K., D. A. Roberts, M. L. Goldstein, S. Ghosh, and W. T. Stribling (1996), A numerical study of the nonlinear cascade of energy in magnetohydrodynamic turbulence, *Journal of Geophysical Research (Space Physics)*, *101*, 21,619–21,626, doi:10.1029/96JA01773.

Wang, Y.-M., N. R. Sheeley, Jr., and N. B. Rich (2000), Evolution of coronal streamer structure during the rising phase of solar cycle 23, *Geophysical Research Letters*, *27*, 149–152, doi:10.1029/1999GL010698.

Williams, L. L. (1995), Heat Flux and Viscosity of Protons in the Collisionless Solar Wind, *The Astrophysical Journal*, *453*, 953, doi:10.1086/176455.

Willson, R. F., S. L. Redfield, K. R. Lang, B. J. Thompson, and O. C. St. Cyr (1998), First VLA Observations of Nonthermal Metric Bursts Associated with Coronal Mass Ejections Detected by the Solar and Heliospheric Observatory, *The Astrophysical Journal, Letters*, *504*, L117.

Woo, R., and J. W. Armstrong (1979), Spacecraft radio scattering observations of the power spectrum of electron density fluctuations in the solar wind, *Journal of Geophysical Research (Space Physics)*, *84*, 7288–7296, doi:10.1029/JA084iA12p07288.

Woo, R., J. W. Armstrong, M. K. Bird, and M. Patzold (1995), Fine-Scale Filamentary Structure in Coronal Streamers, *The Astrophysical Journal, Letters*, *449*, L91, doi:10.1086/309630.

Yamauchi, Y., M. Tokumaru, M. Kojima, P. K. Manoharan, and R. Esser (1998a), A study of density fluctuations in the solar wind acceleration region, *Journal of Geophysical Research (Space Physics)*, *103*, 6571, doi:10.1029/97JA03598.

Yamauchi, Y., M. Tokumaru, M. Kojima, P. K. Manoharan, and R. Esser (1998b), A study of density fluctuations in the solar wind acceleration region, *Journal of Geophysical Research (Space Physics)*, *103*, 6571, doi:10.1029/97JA03598.

Zlobec, P., M. Messerotti, G. A. Dulk, and T. Kucera (1992), VLA and Trieste observations of type I storms, type IV and pulsations, *Solar Physics*, *141*, 165.